Sensors and Actuators B 267 (2018) 279–293

Contents lists available at ScienceDirect

Sensors and Actuators B: Chemical

journal homepage: www.elsevier.com/locate/snb

An integrated gas-liquid droplet microfluidic platform for digital sampling and detection of airborne targets

Pooyan Tirandazi, Carlos H. Hidrovo *

Department of Mechanical and Industrial Engineering, Northeastern University, 334 Snell Engineering Center, 360 Huntington Ave, Boston, MA 02115, USA

ARTICLE INFO

Article history:
Received 17 October 2017
Received in revised form 13 March 2018
Accepted 13 March 2018
Available online 6 April 2018

Keywords:
Microfluidics
Droplets
Flow-Focusing
Ammonia detection
Digital sampling
Gaseous target

ABSTRACT

The use of microfluidic droplets has become ubiquitous in many Lab-on-a-Chip (LOC) applications ranging from material synthesis to novel biochemical sensing. In this paper, we introduce a new droplet-based approach that incorporates a gas phase for generating liquid droplet microreactors in a microfluidic flow-focusing format. We demonstrate the subsequent on-chip transition, collection and handling of the droplets in a secondary liquid carrier inside a multilayer PDMS structure. The presented technique has potential applications in capturing and probing airborne particles and gaseous vapors using high surface-to-volume picoliter droplets. The discrete microfluidic gas-liquid interfaces created in this approach, greatly facilitate absorption and up-concentration of a gaseous target analyte into the droplet volume. The chip-based format of the units also allows for different microfluidic modules and analytical techniques to be integrated in this platform for droplet probing, providing highly-sensitive LOC detection systems. Here, we demonstrate the basic principles of sample partitioning with gas-liquid droplets by capturing and detection of vaporized ammonia at different gaseous concentrations using Nessler's reaction inside the droplets. The results of this work provide a simple and robust quantification approach for determining gaseous ammonia which can be further expanded to other gas-phase analytes in next generation of airborne target detectors for human breath analysis and environmental monitoring.

1. Introduction

Over the past two decades the concepts of miniaturization and compartmentalization have been extensively incorporated in biochemical experiments for a wide variety of applications. The advent of droplet microfluidics has greatly facilitated many of the technological developments in this regard through generation, manipulation, and processing of libraries of ultra-small fluid microreactors (typically pL to nL volume) at high rates (tens of KHz) [1]. The use of microfluidic droplets offers several advantages over conventional laboratory techniques for performing biology and chemistry [2]. From a physical perspective, due to very high surface-area-to-volume ratios of micron-sized drops, heat and mass transfer rate between each droplet and its surrounding environment are significantly higher which facilitates faster reactions. From a mechanical standpoint, microfluidic techniques have also enabled automated and parallel handling of thousands to millions of digital droplets within a short period of time. Moreover, droplet volumes can be accurately adjusted in this scheme, resulting in a tight control over the distribution of the generated droplets. From a chemical perspective, digitizing a reaction into individual compartments enables precise control over the stoichiometry of an isolated reaction. Moreover, it provides stochastic confinement which increases the concentration of the output signal from a droplets' population [3]. Accordingly, droplet microfluidics has rapidly emerged as an essential component in modern multifunctional Lab-on-a-Chip (LOC) and micro-Total-Analysis Systems (μTAS) for a multitude of applications, namely microbiology [4], polymerase chain reaction (PCR) [5–10], protein crystallization [11–13], single-cell analysis [14], fabrication of functional microparticles [15,16], and drug delivery [17,18].

Droplet formation and entrainment processes are the first steps for utilizing any droplet-based system in applications that benefit from sample digitization. In microfluidics, droplets are typically generated from an aqueous-based liquid in a continuous flow of an immiscible oil (or *vice versa*). In this continuous-flow, emulsion-based technique the two liquids meet at a junction (T-junction [19] or flow-focusing [20]) where individual droplets are pinched off as a result of interfacial tension and shear forces induced by the outer phase [21]. Formation of highly-uniform emulsion libraries has been successfully demonstrated and a variety of methods have been proposed for subsequent manipulation of the droplets for

* Corresponding author.
E-mail address: hidrovo@neu.edu (C.H. Hidrovo).

https://doi.org/10.1016/j.snb.2018.03.057
0925-4005/

mixing [22–24], sorting [25,26], fusion [27–29], and fission [30]. Moreover, advances in microfabrication techniques have enabled planarization of microfluidic systems which enables the design and fabrication of highly complex microchannel networks integrated in a miniaturized LOC platform, capable of performing multiple operations.

Whereas droplet microfluidics has been extensively utilized in a variety of analytical techniques, using a liquid as both dispersed and continuous phases for creation of droplet reactors is considered foundational. Incorporating a gas phase inside microfluidic channels has been mainly targeted towards generation of microbubbles in a liquid flow [31–35] for a range of applications from biomedical ultrasonic imaging [36] to synthesis of micro- and mesoporous structures [37]. However, liquid-in-gas generation of droplets in microfluidic networks is a new approach which has not been practically utilized for any analytical application. The use of a continuous gas flow to form uniform liquid sprays has been demonstrated by placing a capillary tube behind a round orifice plate [38]. In this method, the liquid stream supplied from the capillary tube is drawn by a focusing gas stream discharging through a nozzle into an open environment, forming uniform droplets [39–41]. This technique has been widely applied to the field of material synthesis for creating uniform microparticles [42]. Growth and motion of the liquid slugs inside gas-flow microchannels have been studied for water removal in polymer electrolyte membrane (PEM) fuel cells [43–45]. A few recent studies have also investigated the formation of droplets in confined microfluidic architectures such as the T-junction [46–48], flow-focusing [49–53], and capillary co-flow formats [54]. While these studies have provided useful guidelines regarding droplet generation within enclosed microfluidic channels, tailoring gas-borne droplets for LOC applications has not been shown systematically. In this work, we introduce the new concept of liquid-gas droplet-based LOC systems that involves microfluidic generation of liquid compartments inside a continuous gas flow with capability of subsequent collection and handling of the droplets in a secondary liquid carrier (see Fig. 1). The fundamental idea behind this system is to facilitate sampling of a gaseous analyte through rapid absorption of the target across digital gas-liquid interfaces. We further provide a microfluidic framework for manipulating and processing these gas-based microreactors in the secondary liquid carrier.

To utilize microdroplet reactors in this approach, a number of operations should be realized first. The fundamental characteristic of this technique requires liquid droplets to be created within a continuous gaseous phase. In this stage, droplets with high surface-to-volume ratio can be used to capture and up-concentrate a trace vapor analyte or an airborne pathogen through diffusion of the target into the picoliter volume of discrete droplets. For subsequent collection and handling of the drops the use of a secondary liquid carrier is inevitable as the droplets cannot be incubated within a gaseous phase. An intermediate continuous-phase-exchange process is thus, an integral part of this system. For this purpose, the gas-based generation module is integrated with an on-chip droplet collection unit containing a secondary liquid phase. The architecture of the proposed platform allows for replacing the initial gas-based continuous phase with a secondary liquid-based carrier. For interrogation of the droplet content, they should be in a sequential array moving inside microfluidic channels. As such, a manipulator structure is also embedded in the platform for harvesting and preparing the droplets in such consecutive format for any processing operations. All the mentioned steps are performed within a single multilayer LOC platform. The actual prototype is fabricated and tested using lithography-based methods with Polydimethylsiloxane (PDMS) as the structural material bonded to glass slides. We characterize some of the metrics associated with this platform from the generation stage to the final harvesting of the droplets. The impact of the gaseous flow on the volume of droplet microreactors and their monodispersity is investigated here. Moreover, the efficiency and rate of droplet entrainment during each operation are quantified. In the last section, we demonstrate the practical use of the presented droplet-based approach for detection of vaporized ammonia (NH_3). Known concentrations of ammonia are tested as the carrier gas which is absorbed and mixed within the liquid droplets that contain Nessler's Reagent. Due to the color change of the droplets, the presence of ammonia can be verified and further quantified from the droplets' library. With the current configuration of the microchannels, we could detect down to 500 ppm concentrations during sub-second exposure of the droplets to the trace vapor.

The process presented herein provides many opportunities for next generation of LOC devices suitable for capture and detection of airborne targets. Collection and monitoring airborne particles and gaseous vapors have potential applications in health care, air quality assessment, and real-time screening of chemical reactions [55–57]. The architecture of this platform enables a variety of analytical techniques to be used in such applications with high resolution and sensitivity. One potential example includes performing digital droplet PCR (ddPCR) amplification on captured aerosol samples. Implementing conventional PCR methods in aerosol sciences has emerged in recent years thanks to their enhanced sensitivity and detection time compared to culture-based methods [58–60]. However, as of today ddPCR, in its fundamental level, relies on water-in-oil emulsion droplet technology. Furthermore, since on the same volumetric basis, typical concentrations of airborne microorganisms are several orders of magnitude less than waterborne microorganisms [61], sampling and preconcentrating gas-based targets are key yet challenging tasks to be undertaken prior to any detection procedure [62,63]. Through the use of microfluidic gas-liquid interfaces [64], efficient transport of the samples from the gas into isolated droplets' volumes can take place. Integrating gas-liquid digital microreactors with microfluidic manipulation strategies presented here, makes this scheme

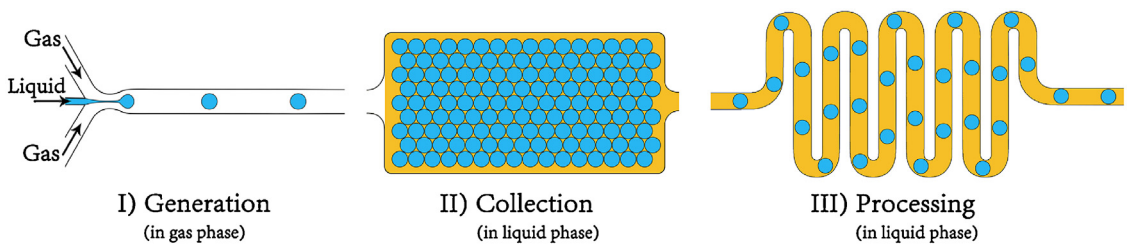

Fig. 1. Conceptual illustration of the process flow in the presented microfluidic approach. I) First, droplets are formed within a continuous gaseous flow. The generated droplets are then carried along the microchannel and are transferred into a second immiscible liquid medium at the exit of the generator unit. II) After transition into the liquid carrier, droplets are collected in an on-chip collector unit. III) Finally, collected droplets are transferred into a second network of microchannels and are prepared for processing of the droplet's content.

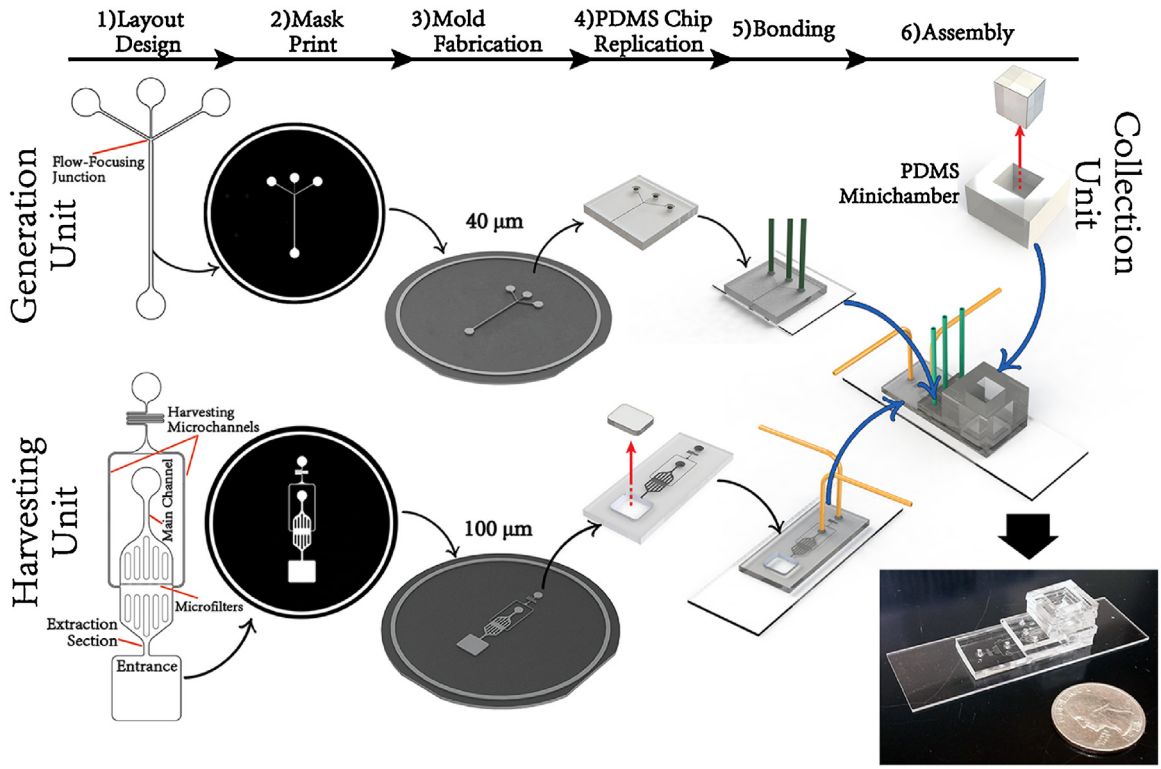

Fig. 2. Schematic diagram showing the fabrication steps of different sections of the platform. For the GU and HU, lithography processes are utilized, whereas the CU chamber is made by cutting of a PDMS slab and forming a hollow structure that eventually sits on top of the GU and HU. The actual platform shown at the bottom consists of a multilayer structure with different units embedded in each layer.

potentially suitable for developing highly sensitive LOC systems which can be used in point-of-care diagnostic breath analysis and environmental monitoring of airborne particulates.

2. Materials and methods

2.1. Device layout and fabrication

The integrated microfluidic platform comprises three main operating units which are referred to as Generation Unit (GU), Collection Unit (CU), and Harvesting Unit (HU). Detailed steps in fabrication of each microfluidic unit are presented in Fig. 2. GU and HU contain microchannels that are fabricated using standard UV lithography processes to create a mold and soft lithography with PDMS for casting the microstructures. GU is composed of a flow-focusing configuration in which a middle dispersed liquid channel meets two side gas flow channels, leading to the generation of droplets. The microchannels are designed in a CAD software and printed out on high-resolution transparencies (CAD/Art services, Inc). Single side polished Silicon (Si) (University Wafer) is used to fabricate a master mold using photolithography process with a negative near-UV photoresist (SU-8 2050 Microchem Corp.). The Si wafer is spin-coated with the photoresist (40 µm thickness), then baked for solvent removal and exposed to UV light through the printed mask. The exposed wafer is then post-baked and developed to obtain a master mold containing the microfeatures. Once the mold fabrication is complete, microfluidic chips are casted out of the SU-8 master mold by performing standard soft lithography method. PDMS prepolymer mixture (Sylgard 184, Dow Corning) is prepared from the elastomer base and curing agent at a 10:1 wt ratio. The solution is then poured onto the Silicon mold, and the assembly is cured at 80 °C for approximately 2 h. Hardened PDMS is peeled off the mold and each microfluidic chip is removed from the PDMS layer. After punching the required flow inlets/outlets, the chip is bonded to a pre-cleaned standard microscope slide (Thermo Scientific) using an oxygen plasma cleaner (Harrick Plasma).

For the HU, a separate layout is designed that comprises different sub-units which we refer to as (i) extraction section, (ii) microfilter, (iii) main channel, and (iv) harvesting microchannels. In the extraction section droplets enter a V-shaped expansion to reduce the spacing between individual drops and create an array of closely-packed digital microreactors. Downstream of the HU, two outlet ports are designed to separate the carrier oil and the droplets. The carrier liquid is removed from the main channel while side harvesting channels separate the droplets. An arrangement of microfilter posts is also placed in the main channel after the side harvesting microchannels to prevent the droplets from entering the main channel while draining the oil. To fabricate the HU structure, a second mold is prepared with a different photoresist (SU-8 2100, Microchem) and spinning speed to obtain taller channels (100 µm thickness). In addition to the outlet ports, a square piece is also removed from the layer, near the unit entrance, to serve as the bottom of the CU. After bonding the harvesting chip to a second glass substrate, the previously-fabricated generation chip is bonded on top of the harvesting chip. Finally, to complete the structure of the platform, a hardened hollow PDMS slab is prepared and assembled on top of the previous layers. This structure will be prefilled with the liquid carrier and is designed to remove the gas bubbles from the open top of the CU while retaining and collecting the droplets at the bottom of the CU. All these units are packed into an integrated multilayer structure. The assembled device is placed on a hot plate for several hours at 200 °C to enhance the bonding strength of the layers. The post-bake process also allows for PDMS microchannels to regain their intrinsic degree of hydrophobicity [65] which greatly facilitates generation and entrainment of aqueous droplets within both gaseous and liquid (oil) carriers of the system.

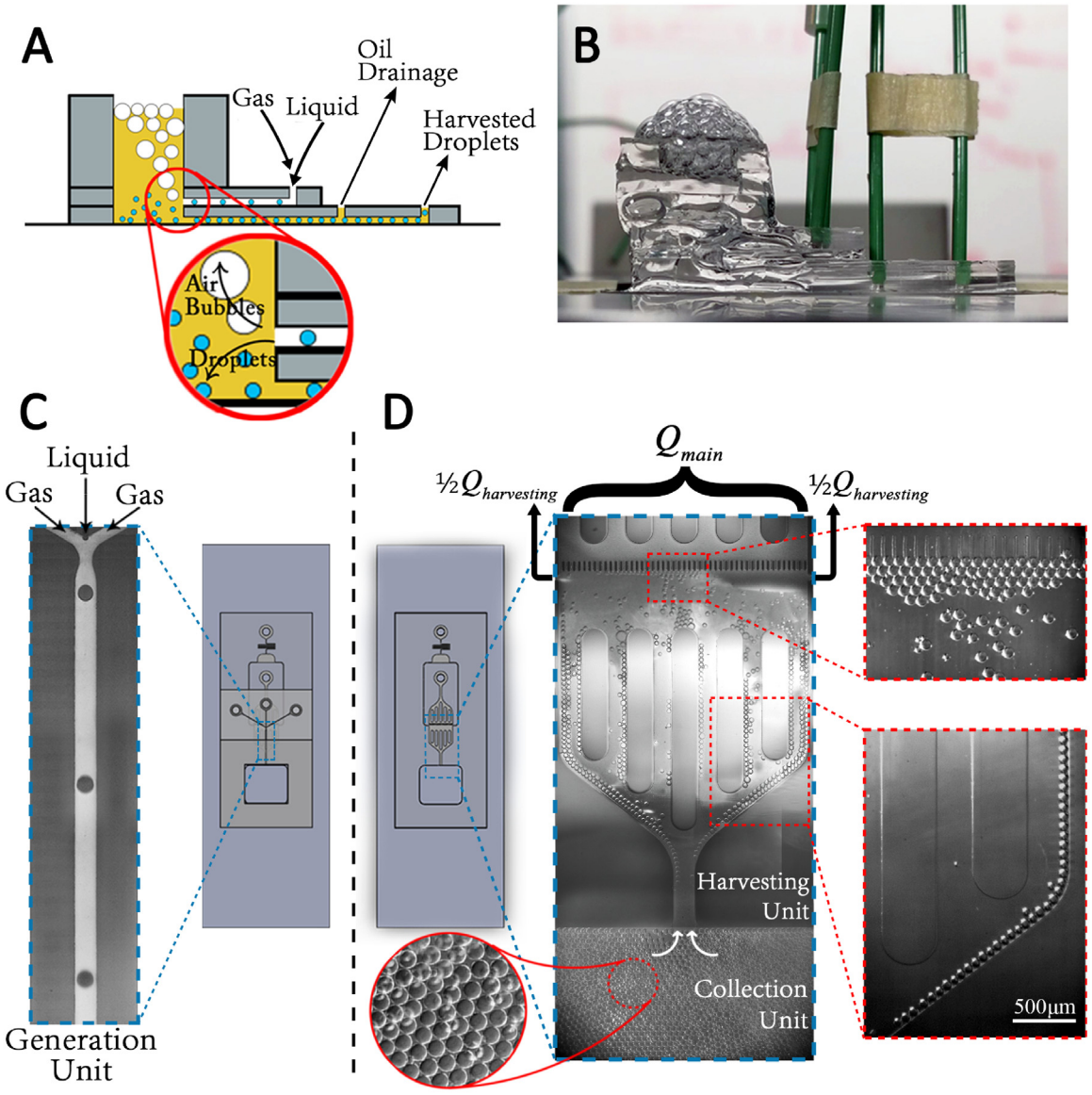

Fig. 3. (A) Schematic and (B) actual images of the operation principle of the platform (side view). The outlet of the GU feeds into the oil bath where the droplets are collected in this immiscible liquid accumulating at the bottom of the CU. Concurrently, the gaseous phase is separated from the droplets as it leaves the CU in the form of bubbles. (C) Operation procedure of the GU; droplets are formed in a flow-focusing junction where two side air flows meet the liquid and pinch off the droplets. (D) Operation procedure of the HU; The HU is connected to the CU and pulls in the collected droplets by means of the withdrawal action of the syringes. The droplets enter the extraction section of the HU in which they form packed arrays on the sides while the carrier oil travels through the center of the channel. Downstream of the HU the flow is divided into a main channel flow (Q_{main}) for removing the carrier oil and a pair of side microflows ($Q_{harvesting}$) for harvesting the droplets. A Microfilter array is also placed in the main channel aimed at retaining the droplets while draining the carrier liquid. By adjusting the flow rates of the two paths, the droplets and the carrier liquid are optimally separated and the droplets can be used for further processing operations.

The concurrent operation of the units is shown in Fig. 3 and Multimedia Component 1 (supplementary data). For operation of the device the gas phase is initially introduced in the microchannels of the GU. The CU is then filled with the oil medium to completely cover the outlet of the GU and the HU microchannels are also primed with the carrier oil. Finally, the liquid dispersed phase is injected into the GU. Droplets are generated as a result of the high-speed gas flow and subsequently move with the gaseous carrier along the unit outlet. As the droplets reach the end of the GU, the continuous gaseous phase forms air bubbles as it enters the CU. Because of the difference in relative densities of the generated droplets ($\rho_{droplet} > \rho_{oil}$) and gas bubbles ($\rho_{bubble} < \rho_{oil}$) the liquid droplets are separated from the gas phase at this stage. To facilitate the phase-exchange process from the gaseous carrier to the liquid carrier, the outlet of the GU should be connected to the CU at a higher level in comparison to the inlet of the HU. Experiments show that placing the GU as the bottom layer results in subsequent interaction of the air bubble and the liquid droplets inside the CU that could substantially affect the droplets' population after collection. However, placing the GU at a higher level from the platform base, allows for the droplets to gradually sink at the bottom of the CU without much interaction with the gas bubbles. As the droplets accumulate at the bottom of the CU, they enter the HU due to an induced flow from pulling syringes that brings in the created emulsion comprising the collected droplets and the oil carrier. Inside the HU, droplets are initially packed in the V-shaped extraction section on the sides of the microchannel (see Multimedia Component 2 in the supplementary data). Subsequently the oil is extracted from the emulsion through the main channel while the droplets are retained and prepared for subsequent interrogation operations in harvesting

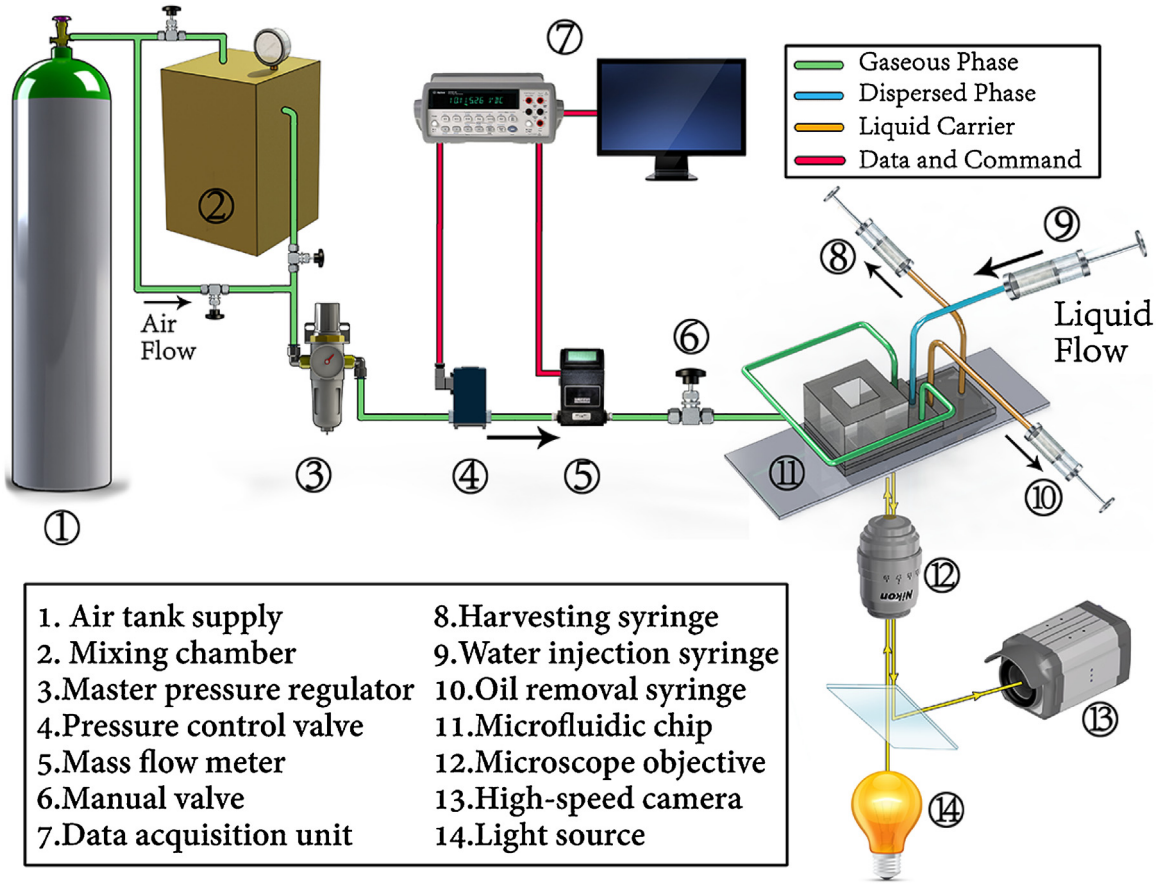

Fig. 4. Experimental setup for control and monitoring the gas and liquid flow into the microfluidic platform. For the characterization of the platform, dry air is directly injected into the platform as the continuous gas phase. For the proof-of-concept, a mixture of ammonia is used as the continuous gas which is prepared in a chamber upstream of the microfluidic platform.

microchannels. This is achieved using a cross-flow scheme where two independently-controlled flows (Q_{main} and $Q_{harvesting}$) manipulate the droplets population and the carrier oil to travel in separate routes.

2.2. Experimental procedure

A custom microfluidic test bench, shown in Fig. 4, is developed to facilitate simultaneous liquid-gas generation and liquid–liquid handling of droplets for all the units. For the GU, gas flow is supplied from the facility compressed air line and is first dried and filtered through a desiccator. A manual regulator (0–150 psi) followed by a voltage-controlled valve (0–20 psi) (Proportion-Air Inc.) reduce the pressure to the operational range of the device. A mass flow sensor (Sierra Smart-Trak2) is also placed in the route of the gas for measuring the rate of incoming gas flows. The control valve and the sensors are connected to a host computer where a customized LabVIEW interface is used for real-time user control as well as data acquisition. For the proof-of-concept experiments, an intermediate blending chamber is placed in the air route. The purpose of this chamber is to prepare a gaseous ammonia sample with a known concentration and inject it into the device. Multiple manual valves are thus placed in the line to easily switch between the dry air and ammonia mixture lines if needed. All the liquids are loaded in individual glass syringes and are controlled using constant displacement syringe pumps (Harvard Apparatus). For the GU, a single line is used to inject the dispersed liquid into the device. Two individually-controlled syringes operating in the withdrawing mode are connected to the HU for controlling the removal rate from the HU. Visualization and imaging is done by a high-speed CMOS camera (Photron SA5) coupled with an inverted microscope (Nikon Ti-U). Illumination is provided by a metal halide white light (Prior Scientific).

DI water is used as the dispersed phase and dry air as the continuous phase for the platform demonstration. The carrier liquid for droplet collection and harvesting is composed of Hexadecane and 3 wt% of a nonionic surfactant (Span 80) (Sigma Aldrich Corp.). For the proof-of-concept, ammonia is introduced in the gaseous phase which acts as a trace vapor. The vapor mixture is prepared by evaporation of 30% ammonium hydroxide solution (NH_4OH, Sigma Aldrich Corp.) in a confined pressurized air chamber. We added 50% of Nessler's Reagent (NR) (Hach Company) to the dispersed water phase as the detection solution. The reaction between NR and the gaseous ammonia results in a color shift of the droplets that was used to probe the ammonia in the gaseous mixture.

3. Results and discussion

3.1. Droplet generation and collection

Droplet formation and breakup in liquid environments are vastly studied in the literature [66–71]. It has been shown recently that droplet generation in gas microchannels can also occur in similar well-known regimes, such as dripping and jetting which are the two most preferable modes for controlled sample digitization [49,50,53]. Due to high viscosities and low velocities of the liquids involved in the microchannel, the Reynolds number (*Re*), which compares the relative importance of inertia to shear forces, is typi-

cally small in liquid-based microfluidic systems ($Re \leq 10$) [72]. Thus, with the viscous stresses dominating the flow, droplet generation is presumed to occur in an inertia-less medium [73] allowing for highly predictable flow dynamics inside the microchannel. Consequently, generation process can be effectively manipulated for creating uniform droplets. Having a low-viscosity gas phase as the continuous fluid necessitates much higher flow speeds to provide adequate force during droplet breakup process. Although the continuous gas phase has a lower density in comparison to a typical oil phase, higher speeds and lower viscosities all result in bigger gas Reynolds number (Re_G) during droplet generation. For this system, we define Re_G as;

$$Re_G = \frac{4\rho Q_G}{\pi \mu D_{ch}} \quad (1)$$

where ρ and μ are the air density and viscosities at room temperature. Q_G is the measured gas flow rate inside the channel and D_{ch} is the characteristic length scale (hydraulic diameter) of the GU outlet. Re_G for the dripping regime ranges from 10^1 to 10^3. Therefore, inertia effects become more relevant and prominent in the performance of this system. In contrast to the liquid–liquid systems, experimental observations of liquid-gas droplet generation in this system shows a more delicate and unstable dripping behavior due to the high-speed flows around the liquid thread. We investigate the influence of Re_G on two important parameters; first, the volume of the generated droplets under different Re_G and second, the population distribution of the droplets. Experiments are conducted for different flow rates of water (dispersed phase) and air (continuous phase) within the dripping region of the GU. The droplets were generated in the gaseous medium and transferred and collected within the immiscible liquid medium in the CU. We performed the measurements of droplet volume and distribution in the collected stage using a custom MATLAB script to analyze droplet population. Fig. 5 shows the trend of the droplet volume for different Re_G and liquid flow rates. Generated droplets in this system contained sub-nanoliter volumes. It can be seen that as Re_G increases higher inertial forces create smaller droplets during detachment process. Droplet volume however, does not exhibit any apparent dependence on the liquid flow rate. Thus, the volumes can be expressed as a function of Re_G in this system.

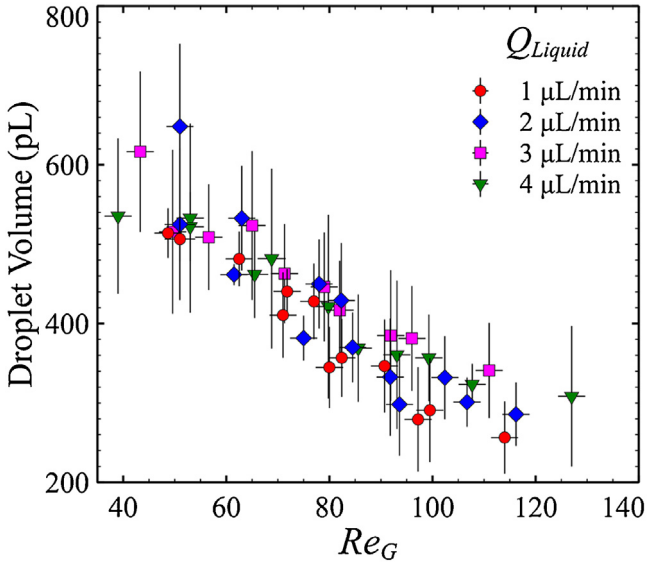

Fig. 5. Volume of the generated droplets in the dripping regime under different liquid and gas flow conditions. Droplet volume is mainly dependent on the gaseous phase and decreases by increasing the gas Reynolds number (Re_G). The error bars for the volume represent the uncertainties of the average droplet volume over multiple experiments.

It is worth noting that although higher Re_G substantiates the role of inertia in the breakup dynamics, it does not mean that viscous induced forces are completely negligible. Direct viscous-based shear stresses at the droplet interface are relatively small and insignificant in the droplet breakup. However, forces induced by hydrodynamic pressure differences arising from viscous gas flow confinement in the microchannel can be quite relevant. This becomes apparent by looking at the ratio of *Re* to *Po* (Poiseuille) or *fRe* number, which is calculated to be in the order of unity for this system, reflecting the non-trivial and in some cases significant role of this viscous induced force in the breakup. As such, droplet breakup in the dripping regime is caused by a combination of surface tension, viscous-based hydrodynamic pressure, and inertial-based drag [49].

The high speed gaseous flow also impacts the monodispersity of the generated droplets. The results of droplet distribution as a function of Re_G are shown in Fig. 6. We can see that as the Re_G increases, droplet population becomes less monodisperse. We think these changes stem from two phenomena. Upon increasing Re_G, inertial effects of the gaseous stream severely impact the liquid thread during formation of the droplets and result in the creation of smaller satellite droplets. Thus, at higher Re_G (>100) droplet population shows a bidisperse distribution consisting of original droplets and smaller daughter droplets. The second influence of the gas phase occurs in the process of transitioning from the GU to the CU. Since droplet movement inside the GU happens at relatively high velocities (≈1 m/s), transitioning into the liquid medium can possibly occur by high speed impact of the droplets with the oil interface. Moreover, physical interaction of the generated bubbles in the CU with the liquid droplets can cause secondary droplet breakup inside the liquid medium. We could not experimentally track each droplet during transition into the CU. Therefore, we considered the combined efficiency of the generation and transition processes in terms of droplet polydispersity index (PDI) defined as σ/d (where σ represents the standard deviation of the droplet diameters and d is the average diameter of the generated drops). It can be seen that droplets with narrower distribution can be obtained at lower Re_G, whereas wider distribution is observed as the Re_G increases. Distribution of the drops represent a PDI of less than 5% at lower values of Re_G (Re_G<60) and up to 20% at higher Re_G values (Re_G>100). Hence, although increasing the Re_G results in smaller size droplets, it may also contribute to polydisperse generation. This attribute is highly critical for precise control of reaction stoichiometry inside individual droplet volumes and improvement of the accuracy of the results in LOC applications. Furthermore, generation of microparticles and microcapsules for drug delivery systems also requires precise and predictable volumes of the drug into the body which necessitate highly uniform droplets with very low variations in size.

In addition to the flow conditions, microfluidic generation of droplets in confined microstructures highly depends on the geometry of the system. Planar flow-focusing configurations provide a versatile scheme with multiple geometrical parameters to control the generation process for obtaining the desired droplet size and generation rate [74]. In the present study, we do not intend to investigate the detailed role of the geometry on the droplet formation. The goal of this section is to enhance the performance metrics of the GU to create smaller yet monodisperse droplets. In confined microfluidic channels, droplet sizes are scaled with the microchannel dimensions. In the case of a continuous liquid phase, since the flow rate of each stream is controlled, reducing the dimensions of the outlet channel leads to higher fluid velocities which induce higher tangential stresses on the dispersed liquid thread at the junction. Consequently, smaller threads are formed from which smaller droplets will be emitted. The same argument also

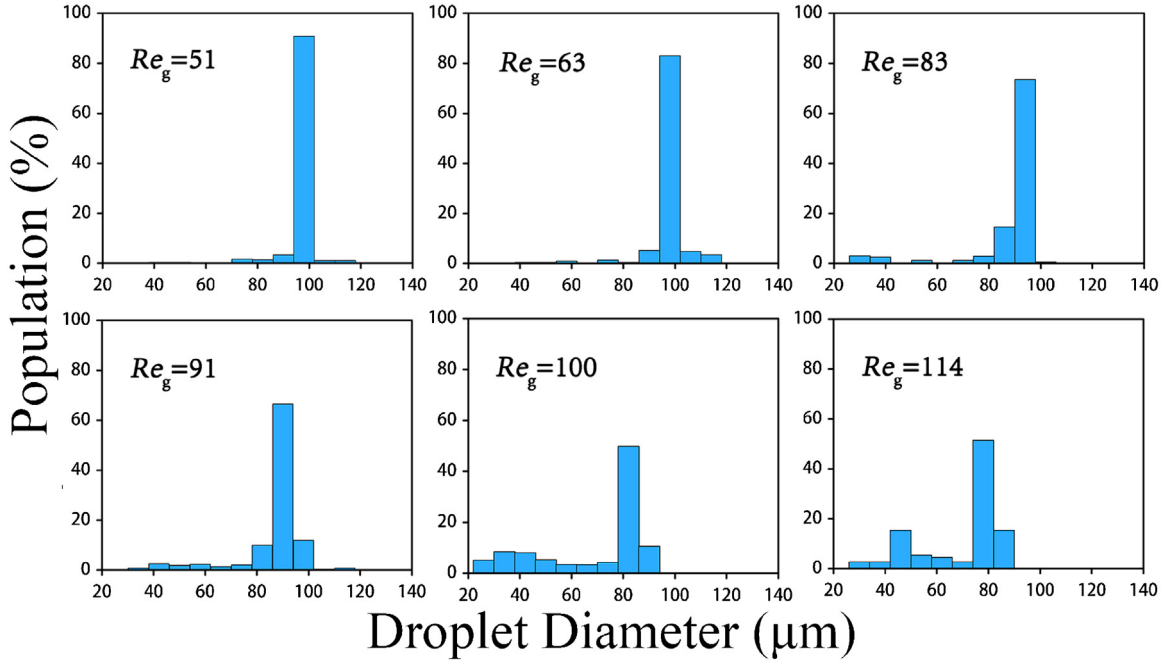

Fig. 6. Distribution of the collected droplet sizes under different Re_G. Highly monodisperse droplets can be obtained at moderate Re_G. Increasing the Re_G causes satellite droplet generation which adversely affects the monodispersity.

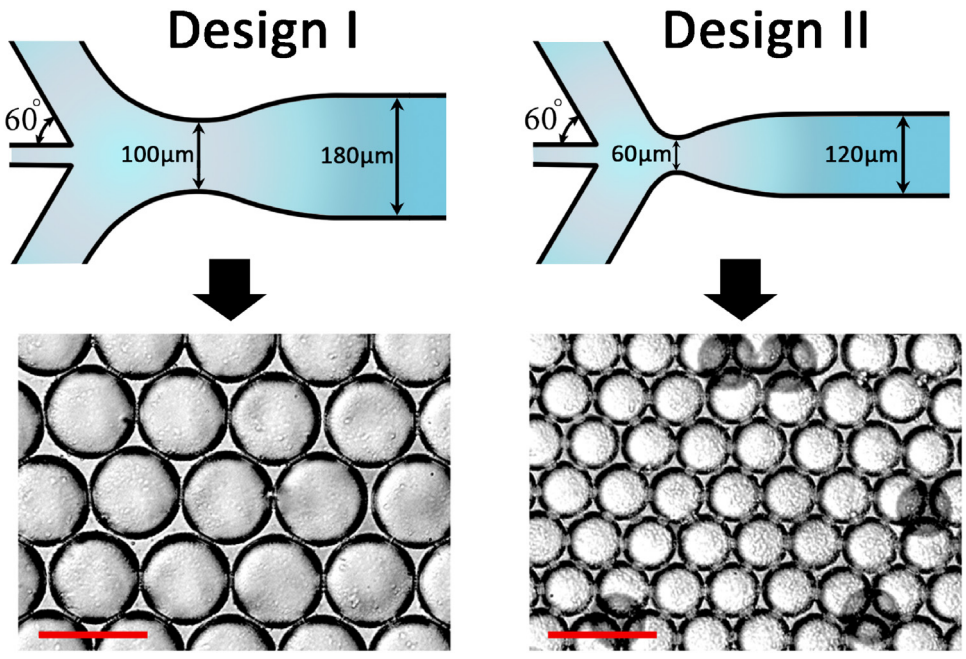

Fig. 7. Schematic of the two microchannel designs of the GU used for droplet generation (Top). Microscopic images of the collected droplets for each configuration under similar flow conditions (Bottom). The scale bars show 100 μm in both images.

applies for this system. For the same gas flow rate that corresponds to the dripping mode of the system, the velocities become higher in the channel which result in higher inertia forces at the junction and smaller droplets. Moreover, due to increased channel resistances, obtaining the appropriate flow rate for the dripping regime requires higher inlet pressures. Increased pressure of the gaseous flow also creates bigger normal stresses which can contribute to reducing droplet size after detachment. The junction of the flow-focusing channel is also a key element affecting both the flow field and the forces involved in the breakup process. Introducing a converging-diverging section induces a favorable hydrodynamic pressure drop across the emerging droplet which facilitates droplet detachment [49]. Shrinking the converging section of the junction causes a higher hydrodynamic pressure force exerted on the liquid thread which creates smaller threads and resultant droplets. Each configuration and the resultant droplet population collected in the CU are shown in Fig. 7. Droplet size and generation frequency are compared for two designs with 180 μm (Design I) and 120 μm outlets (Design II) in Fig. 8. Reducing the channel width proportionally reduces the size of the generated droplets in the GU. Consequently, since the product of droplet volume and generation frequency corresponds to the dispersed liquid flow rate, for the same liq-

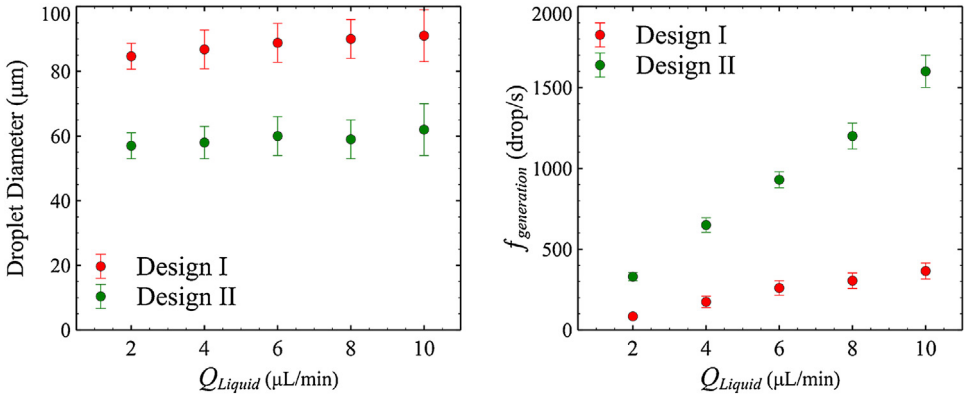

Fig. 8. Comparison of the performance metrics for the two microfluidic chip designs. Design II contains a narrower junction and outlet channel in comparison to Design I. Reducing the microchannel dimensions facilitates generating smaller uniform droplets and consequently increasing the rate of the generation for the same flow inputs.

uid flow conditions, generation frequency increases. We were able to obtain highly monodisperse droplets with a mean diameter of 55 μm at more than a kilohertz formation rate by modifying the microchannel geometry. It should be noted that, while decreasing the microchannel dimensions results in better performance, it would substantially increase the required gas pressure to flow the air into the system which is experimentally challenging to control in the channel. Moreover, reducing the channel width also reduces the gap between the side walls and droplets which increases the possibility of microchannel wetting. We observed that the generated droplets under such high pressures (P_{air} > 15psig) in smaller channel sizes (80 μm) showed highly-unpredictable behaviors and in most cases formed a liquid spray inside the channel. Under such pressures in microscale dimensions, noticeable compressibility (Fanno flow) effects are highly possible which add further complexity in the interactions of the flows.

3.2. Droplet harvesting

Since the collection chamber features miliscale dimensions which holds a prefilled oil solution (1–5 mL), droplets population exist in very small droplet-to-oil volume fractions. Conventionally, droplets are collected in an off-chip reservoir and re-injected into separate microchannels for subsequent processing and screening operations. However, such procedures are prone to human errors and incubation issues which reduce the efficacy of the entire process. Therefore, automated handling of droplets in conjunction with the generation and collection steps is necessary for creating an integrated LOC platform. By having the droplets collected inside the platform, we implement a pressure-driven microfluidic scheme for extraction of the droplets from the CU and drawing off a controlled portion of the oil phase from the emulsion. A key factor in the design and performance of the HU is the size of the unit entrance. Using PDMS replicas are prone to a number of drawbacks arising from the softness of the material. Stability of the PDMS structures is a common concern which has been previously reported in the literature [75]. Due to the elastic nature of the PDMS, recessed microchannel structures undergo natural deformation of the top wall commonly known as “sagging” [76,77]. As the width-to-height aspect ratio of the cross section increases, this deformation can lead to complete collapse of the channel at the central regions. Moreover, since the withdrawing operation of the syringes induces a suction inside the unit, inward flow-induced deformation can also act as a drawback [78]. Swelling of PDMS networks when exposed to certain solvents is another well-known phenomenon which occurs over time as the porous network absorbs the oil [79,80]. A combination of these physical and chemical phenomena causes expansion of the walls and their protrusion into the microchannel. This diminishes the area, especially in the middle regions of the entrance. Consequently, collected droplets are mostly extracted from the narrow openings near the side walls. This led to shear-induced droplet splitting at the channel entrance due to high velocities and shear stresses experienced in the small opening of the entrance. We experimentally investigate the optimal size of the entrance channel to reduce the possibility of droplet breakup during the extraction process. To mitigate the swelling, we also adopted some of the previously-reported strategies, namely reducing the ratio of the PDMS to curing agent as well as thermal treatments [81]. Three channel widths (4700 μm, 1200 μm, 400 μm) are fabricated separately for the HU entrance. The performance of extraction process is assessed in terms of the extraction efficiency ($\eta_{extraction}$) which is defined as:

$$\eta_{extraction} = 1 - \frac{N_B}{N_T} \tag{2}$$

where N_T represents the total number of the extracted droplets over a certain amount of time and N_B is the number of drops that were broken into smaller compartments after entering the HU. Fig. 9 shows the change in the extraction efficiency over time as a result of gradual collapsing of the microchannel. Since the efficiency shows a time-dependent behavior, we believe microchannel swelling has the major contribution for this particular extraction flow rate. By reducing the width of the entrance however, the amount of collapsing becomes less and almost no droplet splitting occurs during the extraction (See Multimedia Component 3 in the supplementary data). It is worth mentioning that we found a certain amount of sagging beneficial for the extraction process. The difference in the channel height due to the wall deformation creates a cross section where droplets are only able to enter the channel from the sides, whereas the oil carrier is allowed to enter from the center of the entrance that has smaller height. Therefore, a pre-separation of the droplets and the oil medium can be achieved during the extraction process by forming a chain of droplets on the side walls, which facilitated subsequent droplet harvesting.

Two different entrance configurations are compared in terms of droplet extraction rate from the CU. The extraction rate ($f_{extraction}$) is directly calculated by manual counting of the entered droplets in a specific time interval. Fig. 10 shows the performance of the two systems as a function of $Q_{extraction}$ which is the sum of the two induced flows from the syringes. In the first case, a single entrance similar to the previous section with maximum $\eta_{extraction}$ is used. The second configuration features six equally-sized parallel entrance units. Both devices are connected to a pair of outlets for oil drainage and droplet harvesting and are tested under same flow rates. The negative values used for the flow rates in the plot represent the withdrawal nature of the extraction. The results of

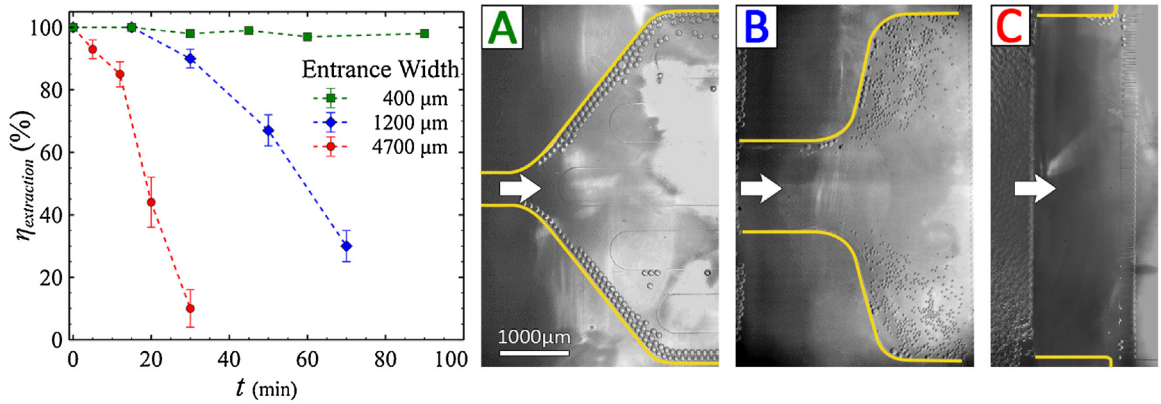

Fig. 9. Experimental data comparing the impact of the entrance channel size on the extraction efficiency ($\eta_{extraction}$) for (A) 400 μm entrance, (B) 1200 μm entrance, and (C) 4700 μm entrance. $\eta_{extraction}$ is defined as the ratio of the number of droplets that are extracted without splitting at the entrance, to the total number of the droplets that enter the HU. The collected droplets for all the three cases are generated under the same water and air flow rates, and thus, have the same average size before entering HU (≈100 μm). However, in wider entrances (case B and C), due to high deformation of the PDMS channel wall, the entrance area is substantially blocked and as a result, droplets split into many smaller satellite droplets. By reducing the entrance size, the amount of channel deformation is minimized and unwanted droplet splitting is reduced during extraction. As such, extraction efficiency can be kept at it maximum over time ($\eta_{extraction} \approx 100\%$).

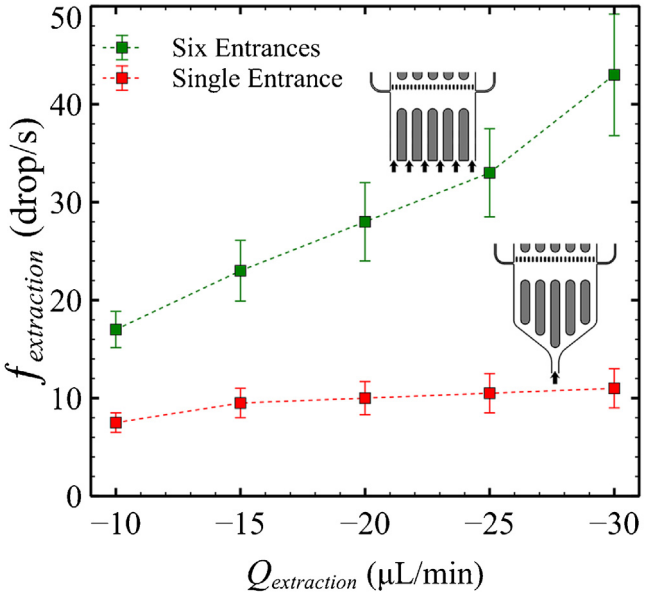

Fig. 10. Comparison of the extraction rate ($f_{extraction}$) between two different entrance configurations. $Q_{extraction}$ is the total volumetric flow rate at which the emulsions (carrier oil and the collected droplets) are extracted from CU and enter the HU. Due to the withdrawal nature of the extraction process, the flow rates are shown in negative values. By increasing the number of entrances, droplets enter the HU in a parallel manner which result in higher $f_{extraction}$.

the six-channel entrance demonstrate an increase of 300% in the extraction rate in comparison to a single entrance. Moreover, since the flow is divided between six channels, for the same flow condition, high shear stresses at the entrance of a single channel can be avoided.

In the main section of the HU a cross-flow configuration is designed to separate the continuous oil carrier from the emulsion and retain the droplets. A microfilter array composed of microscale pillars was designed right behind the intersection of the two side harvesting channels. The spacing between each pair is smaller than the average range of the droplets' diameters to prevent the bypassing of the droplets. The flow in this region is divided between the main channel (Q_{main}) which passes through the filters, and the side harvesting channels (each being $0.5Q_{harvesting}$). To characterize the droplet harvesting, we define and consider an efficiency and rate for the harvesting process as well. Harvesting efficiency ($\eta_{harvesting}$) is defined as:

$$\eta_{harvesting} = \frac{N_H}{N_C} \tag{3}$$

where N_H is the number of droplets that enter the harvesting mirochannels and N_C is the total number of droplets that entered the HU without splitting at the entrance. Therefore, N_C is equal to the difference between N_T and N_B ($N_C = N_T - N_B \approx N_T$) from the extraction process. The harvesting rate ($f_{harvesting}$) is defined as the total number of drops that enter the two harvesting channels over a certain period. In Fig. 11 $\eta_{harvesting}$ and $f_{harvesting}$ are plotted as a function Q_{main} and $Q_{harvesting}$.

From the plots we can see that Q_{main} plays a twofold role in the harvesting rate. Upon initiating Q_{main} the harvesting rate increases. In fact, increasing Q_{main} increases the total number of incoming droplets ($N_C \approx N_T$) which also increases the concentration of the droplets present in the HU. Since the flow streamlines are divided between the main and harvesting channels, upon increasing N_C, more droplets will follow the streamlines to the side channels ($N_H\uparrow$), thus, $f_{harvesting}$ initially increases. Further increase in Q_{main} directs the majority of the flow streamlines towards the main channel which creates a competing situation between the two paths to attract the droplets. As a result, in the plots there is an optimum point for Q_{main} to obtain the maximum value of $f_{harvesting}$ (see Multimedia Component 4 in the supplementary data). The decreasing trend in $\eta_{harvesting}$ also demonstrates the fact that smaller portion of the entered droplets are harvested at higher Q_{main}. At higher Q_{main} trapped droplets behind the microfilters can overcome the capillary pressure in the gap and squeeze through the micropillars. It should be noted that although increasing $Q_{harvesting}$ results in higher $\eta_{harvesting}$ and $f_{harvesting}$, the droplets packing fraction is reduced due to higher oil fractions that enter the side microchannels.

3.3. Ammonia vapor digital sampling

Application of liquid-in-gas droplets is demonstrated here for detection and analysis of vaporized ammonia in a gaseous sample. As a proof-of-concept we picked Nessler's reaction which is the most common coloration reaction for spectrophotometry ammonia detection [82]. The dispersed water phase is mixed with 50% solution of Nessler's Reagent (NR). A mixture of gaseous ammonia in air is used as the continuous phase. Upon exposure to the gaseous mixture, a rust orange precipitate is produced within the droplets

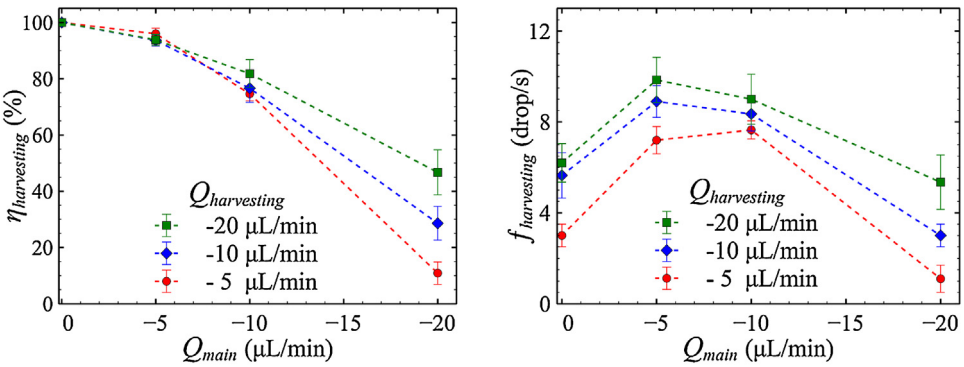

Fig. 11. Experimental data illustrating the harvesting efficiency ($\eta_{harvesting}$) and harvesting rate ($f_{harvesting}$) for different Q_{main} and $Q_{harvesting}$. Since the harvesting process involves withdrawing the liquid carrier, the values are shown as negative numbers. $\eta_{harvesting}$ is defined as the ratio of the number droplets entering the side Harvesting Microchannels over the total number of the droplets that enter the HU, and $f_{harvesting}$ represents the rate at which the harvesting takes place. Increasing $Q_{harvesting}$ has a favorable effect on $\eta_{harvesting}$ and $f_{harvesting}$ as it always increases both the efficiency and the rate of harvesting. By increasing Q_{main} more droplets are extracted from the CU and transferred into the HU. However, this may also lead to losing more droplets as they bypass the microfilters at higher values of Q_{main}. We can see that $\eta_{harvesting}$ consistently decreases with increasing Q_{main} while $f_{harvesting}$ shows a tradeoff representing an optimal point for handling the maximum number of the droplets per second for a given value of $Q_{harvesting}$.

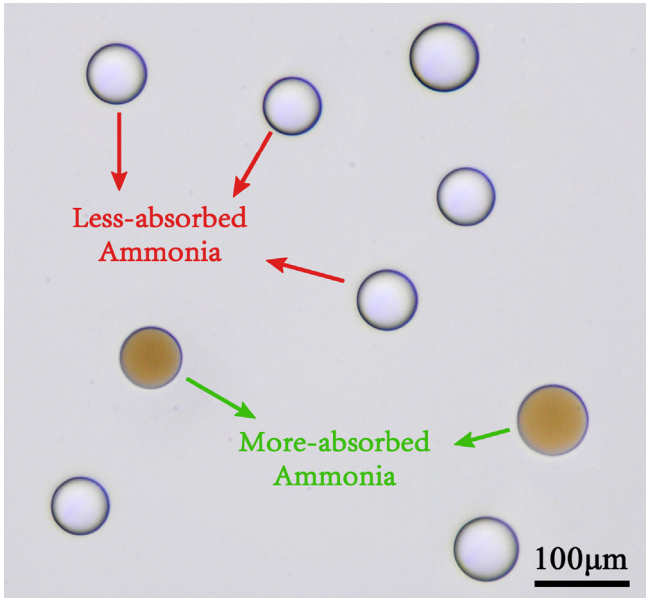

Fig. 12. Color change of the droplets upon exposure to the gaseous ammonia mixture. Here, the inert gas phase is premixed with vaporized ammonia. The mixture is then used as the continuous phase for droplet generation in the GU. Liquid droplets are also mixed with the Nessler's Reagent (NR). During generation and entrainment process, droplets are exposed to the ammonia which chemically react with NR and results in an orange precipitate inside the droplets. (For interpretation of the references to colour in this figure legend, the reader is referred to the web version of this article.)

due to the reaction of the mercury compounds in NR with ammonia (see Fig. 12 and Multimedia Component 5 in the supplementary data). This results in a color shift that is related to the amount of reaction taking place within a droplet, which is in turn proportional to the amount of ammonia absorbed by said droplet.

Using the presented liquid-in-gas droplet microfluidic system provides a multitude of features that make it very intriguing for sampling and analysis of air-based targets. The architecture of this platform allows a gas-phase species to interact with the free surface of picoliter droplets. Throughout the exposure of the droplets to the gaseous flow, from the generation stage and subsequent movement within the GU until their transition into the CU, an airborne target can be absorbed into the droplet volume. This target can be in the form of a vapor or an airborne particulate, which is sampled into individual ultrasmall volumes. As such, the captured targets are tightly confined within each droplet volume, leading to a 100X and above increase in concentration on a mole-per-liter basis as compared to their initial gaseous state. The equilibrium concentration of the gaseous analyte absorbed into the liquid droplets is related to the gas flow pressure in the GU, the partial pressure of the species and its abundance in the gas phase. However, its absorption rate is inversely proportional to the liquid diffusion length scale, and therefore quite large in microdroplets due to their larger surface-to-volume ratios. Fast volumetric up-concentration is the primary advantage of using microdroplets for gaseous sampling.

Mass transfer between gas and liquid in a confined microchannel as in the present architecture involves several physical phenomena that can simultaneously play a role in the droplet dynamics as well as the absorption process. The amount of the absorbed target in the droplets is determined by the interplay of a vast parameter space, including the local gas pressure, flow velocities, droplet size, and the residence time of each droplet in the GU, to name a few. Precise control of all these experimental parameters is almost impossible in practice. Fluctuations in the local pressure during the generation process will not only affect the final droplet size but it would also change the equilibrium concentration between the two phases. Droplets can experience different residence times within the GU due to the variation of air drag force on the droplet which is also a function of *Re*. Conjugate mass transfer from the droplet (*i.e.* droplet evaporation) when exposed to the gas flow should also be taken into account as it affects both the droplet size and the absorption amount. Moreover, the interaction of the microchannel walls with the droplets in this system can complicate the combinatory effect of all the mentioned factors. The final amount of the absorbed target and the up-concentration factor is a function of all of these variables.

A second advantage of using microdroplets, as opposed to just a continuous two-phase microflow sampling scheme, is the ability to perform sample partitioning. Due to inherent fluctuations in the values of the parameters involved in any experimental run, the data obtained from a single or a very small droplet population will be subjected to substantial error and uncertainty in its correlation to the concentration of the target, and might not even predict the existence of it. In other words, for a given experimental run, different droplets produced in this system may vary in the amount of the absorbed target due to temporal variations in the experimental conditions. By probing a large droplet population exposed to the same experimental conditions, we can mitigate these factors through statistical analysis of the whole droplet library. This is a result of the droplets' intensities being dependent on a multivariable process, as described above, and therefore normally

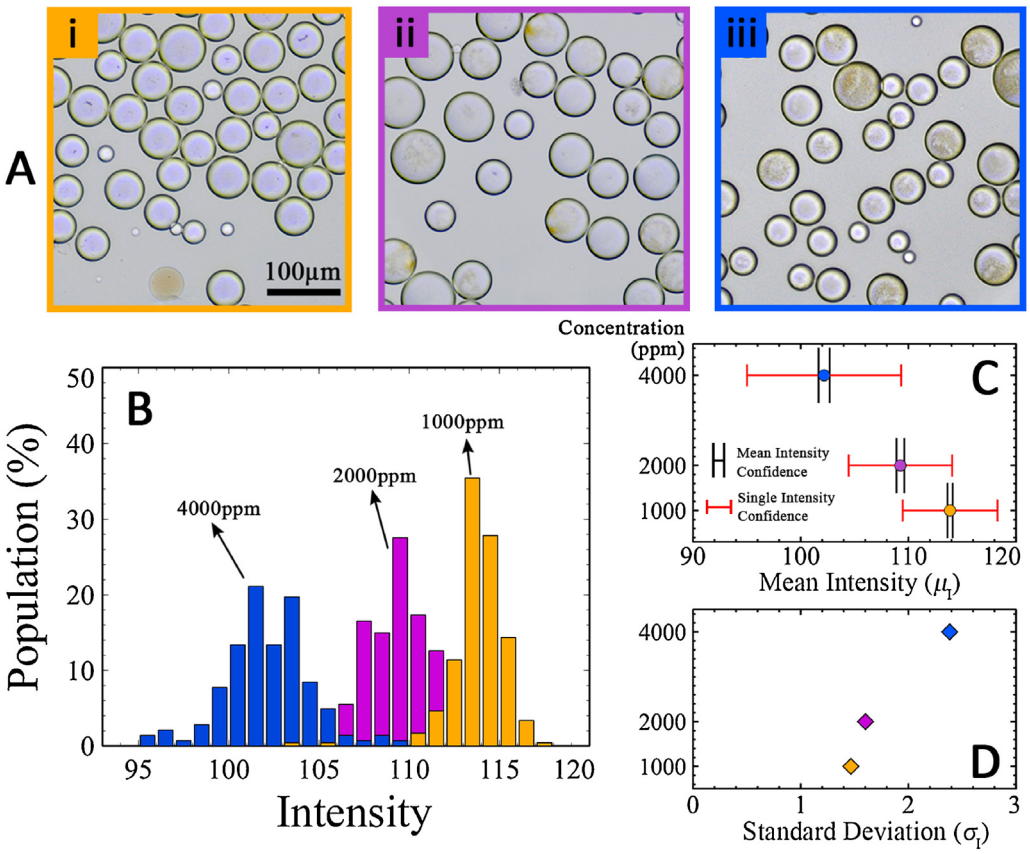

Fig. 13. (A) Images of the collected droplets after exposure to ammonia in the gaseous mixture at (i) 1000 ppm, (ii) 2000 ppm, and (iii) 4000 ppm gaseous concentrations. (B) Comparison of the quantified intensity distribution of each population. Each droplet in the image is assigned with a single intensity value based on the average intensity of the pixels that the droplet comprises. The intensity value is an 8-bit integer ranging from 0 (dark) to 255 (white). Unlike typical fluorescence-based signals, as more ammonia is absorbed into the droplet volume, due to higher amount of the precipitate, droplets become dimmer. Therefore, the intensity distribution shifts to left (lower intensity values). (C) The mean intensity values for each distribution. Confidence intervals are calculated based on%99 confidence assuming a normal distribution for the intensities. The confidence limit for a single data point is $\pm 3\sigma$ while this value for the mean is $\pm z^*\sigma/\sqrt{N}$ where z^* for %99 confidence is 2.576 and N is the total population of the analyzed droplet in each distribution. It is evident that a single data point alone cannot represent a robust measure of the quantified data, whereas considering the mean value of a large droplet library is prone to less errors. (D) Standard deviation of the droplet intensities. The values of standard deviation represent additional information regarding signal differentiation which can be correlated to the gaseous ammonia concentration. (For interpretation of the references to colour in this figure legend, the reader is referred to the web version of this article.)

distributed as prescribed by the central limit theorem (CLT). Sample partitioning of a gaseous analyte *via* a large library of generated droplets provides for three distinct but correlated means of more accurate concentration measurement: (1) reducing the variance by increasing the sample size, (2) extracting additional information by differentiating the signals, and (3) digitizing the overall signals. The idea behind variance reduction is to increase the number of sampled reactions by using several droplets for gaseous target absorption measurements, rather than analyzing a single droplet, providing a more accurate measurement of the concentration. This scheme is inherently more precise and, as will be shown in the results, the average intensity of each droplet population is a more reliable measure of the concentration of the target in the gaseous mixture than a single droplet intensity measurement. Although absorption of the ammonia into a continuous liquid microflow containing NR would also produce an intensity signal similar to that of the average of a droplet population, no information would be provided about the statistical distribution of that signal. Statistical analysis of a partitioned sample in the form of a library of the droplets provides additional information regarding the scattering of the signal in terms of its standard deviation, which is akin to differentiation of a corresponding continuous microflow signal. Last but not least, the statistical distribution of the individual signals from the droplet library is also the basis for the concept of digitizing the overall signal. By defining a threshold on the intensity distribution of the droplets, a positive (high reaction yield and strong color shift) or negative (low reaction yield and faint color shift) value can be assigned to each droplet in the population. This approach provides a simpler and more robust tool for absolute quantification of the signal in a digital format to correlate the target concentration to droplet population count above or below a set threshold.

We performed gas sensing experiments at three different concentrations of ammonia, 1000, 2000, and 4000 ppm. For each case, droplets are generated over a period of 120 s. Random snapshots of the collected droplets after the generation stage are analyzed. To obtain the intensity distribution from the droplet population, the color images are first converted to 8-bit grayscale format (0–255 intensity values) and after identifying the pixels within each droplet, every droplet is assigned with the average intensity value of its constituting pixels. Experimental images of the populations at different ammonia concentrations and their quantified intensity distributions are shown in Fig. 13. As a consequence of the variations in the experimental parameters, the outcoming intensity of the droplets' population would be distributed over a range. As higher concentrations of ammonia are introduced in the gaseous flow, the fluctuations in some of the contributing factors are amplified and the droplets are distributed over a wider intensity range. Moreover, due to higher amounts of the absorbed ammonia, the droplets become darker on average. This happens because of the higher amount of precipitate produced in the Nessler's reaction,

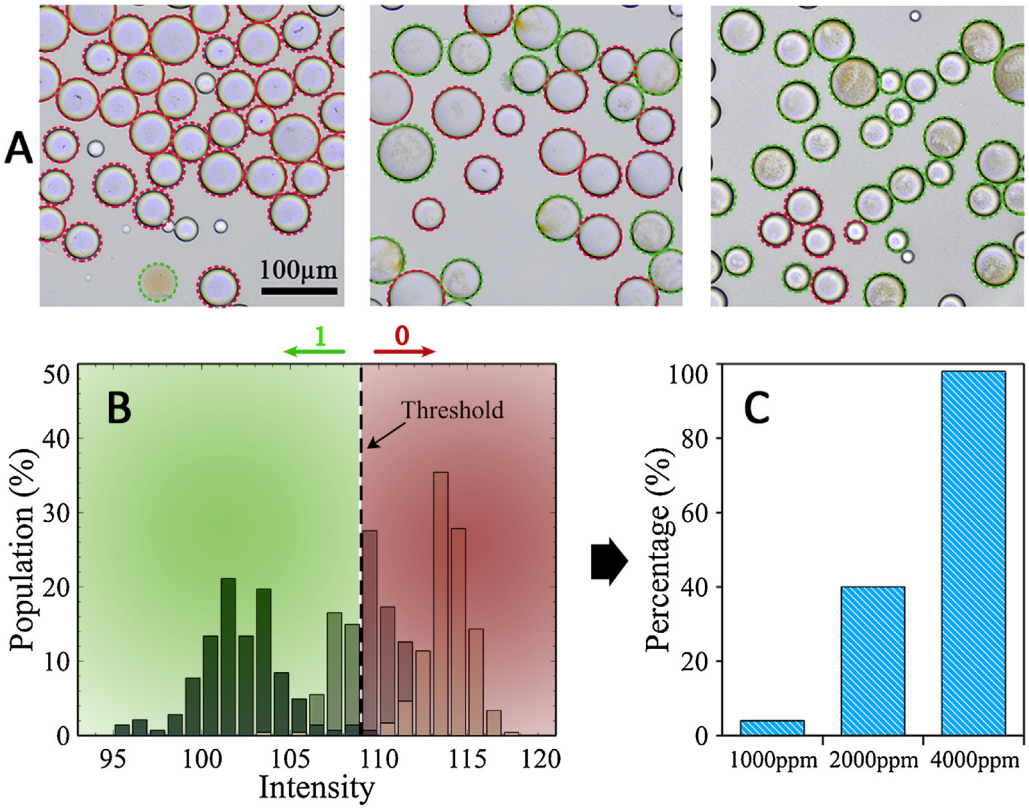

Fig. 14. Digital quantification of the concentration data. (A) The experimental images from the previous part are digitally analyzed with the green droplets representing a strong color change, and red droplets showing a weak color change. (B) By choosing an appropriate intensity threshold the intensity distribution plot can be divided into a digital map where the number of the droplets on the left side are counted as positive signals (green region), and the ones on the right are negative signals that contain little or no ammonia (red region). (C) The percentage of the positive droplets for each distribution is shown in the cumulative bar chart as a measure of the gaseous target concentration. (For interpretation of the references to colour in this figure legend, the reader is referred to the web version of this article.)

which shifts the intensity distribution to the left (lower values). Inhomogeneity of the color within the droplets may stem from several factors, mainly related to the physicochemical interaction of the droplets in the microchannel. Due to the nature of the Nessler's reaction, the contents of the droplets usually form a nonuniform precipitate when exposed to the ammonia mixture. In addition, prior to transition of the droplets to the oil medium, they form a disk-shape morphology in the GU, and are in direct contact with the top and bottom walls while traveling inside the microchannel. Since exposure of the droplets to the ammonia mixture takes place during this period, the gaseous phase does not reach the free surface of the droplets from all sides. Therefore, the absorption and thus the reaction happens non-uniformly at different locations inside the droplet volume. Confinement-induced interactions with the content of the droplets can induce complex advective motions inside the droplets that may either help or worsen the homogeneity of the reaction. Due the change in the properties of the dispersed phase by adding NR to the liquid, droplet generation behavior is altered and unwanted thin liquid films could form on the top and bottom walls as the droplets travel inside the microchannel. Exposure to the ammonia mixture and formation of the rust orange precipitate from the Nessler's reaction can also facilitate the formation of these residues on the walls whose presence are confirmed by experimental images of the microchannel after the Nessler's reaction.

From the intensity distribution of the droplets at different concentrations, it is evident that the data from a single droplet can lie anywhere within its corresponding intensity distribution, which is influenced by the fluctuations in the experimental parameters that affect the absorption amount. Thus, as shown in Fig. 13C determining gaseous ammonia concentration from a single droplet intensity measurement has a large amount of error proportional to the standard deviation, σ_I. However, correlating the gaseous ammonia concentration to the averaged intensity signal of a partitioned sample contains a much lower uncertainty. In fact, the error associate to the mean value is determined by the standard error of the mean (SEM) which is proportional to the standard deviation of the droplet population divided by the square root of the number of samples, $\sigma_I/\sqrt{N}$. Furthermore, by discretizing the intensity signals through the use of multiple droplet partitions rather than a single-partition liquid flow, we also expand the information contained in the signal through differentiation. This additional information from intensity signal differentiation is contained in the value of the standard deviation of the droplet intensities, which can also be correlated to the gaseous ammonia concentration (see Fig. 13D) to improve the accuracy as well as the precision of the overall measurement.

The use of droplets for sample partitioning also allows for the quantification by means of digitizing the data. The idea of digitization, which forms the basis of ddPCR technique for DNA amplification, is to provide a positive-negative (ON-OFF or 1/0) system for signal quantification. By setting up a threshold to determine whether a signal is considered positive or negative, we can express the previous data from droplet distribution in the form of absolute quantification that only considers the droplet count. An example of such quantification is shown in Fig. 14. Here, an appropriate intensity threshold that clearly delineates whether a Nessler's reaction has taken place within a droplet is chosen on the intensity axis. This threshold divides the distribution plot area in two sides. The intensity values above the set threshold (right side) are considered as negative signals which exhibit little or no trace of color change,

while the values lower than the threshold (the left side) are counted as positive signals. This digitization approach lends itself to a cheap, simple, chip-based gas sensor implementation where a relatively inexpensive optical counter device with appropriately set threshold can be integrated in the HU to count the positive droplets for different gaseous concentration values.

We should note that the duration of gas-liquid interaction is a key element affecting the amount of analyte up-concentration inside the droplets, and is directly correlated to the residence time of the droplets inside the microchannel. Experimental observations of the droplet movement inside the GU show that the use of high-speed gas flow for droplet generation creates fast-moving droplets ($V_{droplet} \approx 1$ m/s) in comparison to typical water-in-oil emulsions (≈mm/s). The residence time of each droplet over the course of formation and subsequent movement before being transferred into the CU was therefore measured to be less than one second. With the present architecture, we could detect ammonia concentrations down to 500 ppm. The main focus of this work has been demonstrating the potential of implementing liquid-gas droplets for analytical applications. Future studies of the flow dynamics and the two-phase interactions within confined microchannels is of great consequence as it allows for a better understanding of the phenomena that eventually determine the efficiency of the absorption and consequential gas sensing capabilities of this system. Although some previous studies related to air pollution scavenging using liquid droplets, have considered the internal and external flow dynamics of moving droplets in a gaseous medium and investigated the mass transfer to and from the droplets [83–87], the problem has been mainly considered for a falling droplet in an infinite still air. Investigation of the mass transfer and fluid interactions inside confined gas-liquid environments when a train of droplets are generated and transferred in a microfluidic channel is a novel area that has not been previously addressed, and is open for further investigations. Future studies in this regard may be geared towards investigating and manipulating the gas-liquid interactions for controlling the flow conditions, and optimizing the microchannel geometry to improve the exposure and enhance the device's performance, especially towards lower detection limits.

4. Conclusions

Microfluidic platforms for generation of uniform droplet libraries have become ubiquitous in a multitude of biochemical and diagnostic applications. In this study, we have demonstrated a novel droplet-based platform to generate and manipulate in-gas liquid microreactors. The structure of this platform consists of three units which are Generation Unit, Collection Unit, and Harvesting Unit. The hybrid framework of this technique allows for picoliter liquid droplets to be generated in a gaseous medium facilitating transport of an airborne target across the gas-liquid droplet interface. Subsequently, droplets are transitioned and collected in a secondary immiscible liquid solution where they are entrained and prepared for any processing operations and signal detections. We have demonstrated the practical use of this technique for detection of ammonia compounds in a gaseous mixture through the introduction of Nessler's Reagent into the droplets. The detection has been performed by probing droplets' population as their color shifted due to the reaction of the gaseous ammonia with the droplet content. We have tested three different concentrations in this study, and correlated the gaseous ammonia concentrations to the intensity signals obtained from the droplet library in each case. Although 500 ppm ammonia concentrations are detectable with this approach, further investigations in this regard can be undertaken for controlling the liquid-gas interaction time to enhance the detection limit of this method. Moreover, a variety of analytical techniques can be integrated with the presented liquid-gas droplet system to improve the detection of gas-based targets. We believe many areas related to aerobiology and chemical detections can benefit from this approach towards developing novel LOC systems capable of rapid detection of analyte vapors and airborne particles at very low concentrations.

Acknowledgements

This work has been supported by National Science Foundation (NSF) [grant number 1522841]. The fabrication of the microfluidic devices was possible thanks to the George J. Kostas Nanoscale Technology and Manufacturing Research Center at Northeastern University, Boston, MA. The authors are grateful to Dr. Carlos Rios Perez and Dr. Tae Jin Kim for their helpful assistance regarding the experimental setup and the fabrication process.

Appendix A. Supplementary data

Supplementary data associated with this article can be found, in the online version, at https://doi.org/10.1016/j.snb.2018.03.057.

References

[1] S.-Y. Teh, R. Lin, L.-H. Hung, A.P. Lee, Droplet microfluidics, Lab Chip 8 (2008) 198–220, http://dx.doi.org/10.1039/b715524g.
[2] A. Huebner, S. Sharma, M. Srisa-Art, F. Hollfelder, J.B. Edel, A.J. deMello, Microdroplets: a sea of applications? Lab Chip 8 (2008) 1244, http://dx.doi.org/10.1039/b806405a.
[3] M.E. Vincent, W. Liu, E.B. Haney, R.F. Ismagilov, Microfluidic stochastic confinement enhances analysis of rare cells by isolating cells and creating high density environments for control of diffusible signals, Chem. Soc. Rev. 39 (2010) 974, http://dx.doi.org/10.1039/b917851a.
[4] T.S. Kaminski, O. Scheler, P. Garstecki, Droplet microfluidics for microbiology: techniques, applications and challenges, Lab Chip (2016), http://dx.doi.org/10.1039/C6LC00367B.
[5] V. Taly, D. Pekin, A. El Abed, P. Laurent-Puig, Detecting biomarkers with microdroplet technology, Trends Mol. Med. 18 (2012) 405–416, http://dx.doi.org/10.1016/j.molmed.2012.05.001.
[6] H. Tanaka, S. Yamamoto, A. Nakamura, Y. Nakashoji, N. Okura, N. Nakamoto, K. Tsukagoshi, M. Hashimoto, Hands-off preparation of monodisperse emulsion droplets using a poly(dimethylsiloxane) microfluidic chip for droplet digital PCR, Anal. Chem. 87 (2015) 4134–4143, http://dx.doi.org/10.1021/ac503169h.
[7] M.M. Kiss, L. Ortoleva-donnelly, N.R. Beer, J. Warner, C.G. Bailey, B.W. Colston, J.M. Rothberg, D.R. Link, H. Leamon, R. Technologies, H. Ave, High-throughput quantitative PCR in picoliter droplets, Anal. Chem. 80 (2008) 8975–8981, http://dx.doi.org/10.1021/ac801276c.
[8] Y. Schaerli, R.C. Wootton, T. Robinson, V. Stein, C. Dunsby, M.A.A. Neil, P.M.W. French, A.J. DeMello, C. Abell, F. Hollfelder, Continuous-flow polymerase chain reaction of single-copy DNA in microfluidic microdroplets, Anal. Chem. 81 (2009) 302–306, http://dx.doi.org/10.1021/ac802038c.
[9] N.R. Beer, E.K. Wheeler, L. Lee-Houghton, N. Watkins, S. Nasarabadi, N. Hebert, P. Leung, D.W. Arnold, C.G. Bailey, B.W. Colston, On-chip single-copy real-time reverse-transcription PCR in isolated picoliter droplets, Anal. Chem. 80 (2008) 1854–1858, http://dx.doi.org/10.1021/ac800048k.
[10] P. Kumaresan, C.J. Yang, S.A. Cronier, R.G. Blazej, R.A. Mathies, High-throughput single copy DNA amplification and cell analysis in engineered nanoliter droplets, Anal. Chem. 80 (2008) 3522–3529, http://dx.doi.org/10.1021/ac800327d.
[11] L. Li, D. Mustafi, Q. Fu, V. Tereshko, D.L. Chen, J.D. Tice, R.F. Ismagilov, Nanoliter microfluidic hybrid method for simultaneous screening and optimization validated with crystallization of membrane proteins, Proc. Natl. Acad. Sci. U. S. A. 103 (2006) 19243–19248, http://dx.doi.org/10.1073/pnas.0607502103.
[12] M. Maeki, Y. Teshima, S. Yoshizuka, H. Yamaguchi, K. Yamashita, M. Miyazaki, Controlling protein crystal nucleation by droplet-based microfluidics, Chem. – A Eur. J. 20 (2014) 1049–1056, http://dx.doi.org/10.1002/chem.201303270.
[13] B. Zheng, J.D. Tice, L.S. Roach, R.F. Ismagilov, A. Droplet-Based, Composite PDMS/Glass capillary microfluidic system for evaluating protein crystallization conditions by microbatch and vapor-diffusion methods with on-chip X-ray diffraction, Angew. Chem. 116 (2004) 2562–2565, http://dx.doi.org/10.1002/ange.200453974.
[14] A. Rakszewska, J. Tel, V. Chokkalingam, W.T. Huck, One drop at a time: toward droplet microfluidics as a versatile tool for single-cell analysis, NPG Asia Mater. 6 (2014) e133, http://dx.doi.org/10.1038/am.2014.86.
[15] J. Wang, J.C.T. Eijkel, M. Jin, S. Xie, D. Yuan, G. Zhou, A. van den Berg, L. Shui, Microfluidic fabrication of responsive hierarchical microscale particles from macroscale materials and nanoscale particles, Sens. Actuators B Chem. 247 (2017) 78–91, http://dx.doi.org/10.1016/j.snb.2017.02.056.

[16] W. Wang, M.J. Zhang, L.Y. Chu, Functional polymeric microparticles engineered from controllable microfluidic emulsions, Acc. Chem. Res. 47 (2014) 373–384, http://dx.doi.org/10.1021/ar4001263.
[17] O.J. Dressler, R.M. Maceiczyk, S.-I. Chang, A.J. DeMello, Droplet-based microfluidics enabling impact on drug discovery, J. Biomol. Screen. 19 (2014) 483–496, http://dx.doi.org/10.1177/1087057113510401.
[18] N. Shembekar, C. Chaipan, R. Utharala, C.A. Merten, Droplet-based microfluidics in drug discovery, transcriptomics and high-throughput molecular genetics, Lab Chip 16 (2016) 1314–1331, http://dx.doi.org/10.1039/C6LC00249H.
[19] T. Thorsen, R.W. Roberts, F.H. Arnold, S.R. Quake, Dynamic pattern formation in a vesicle-generating microfluidic device, Phys. Rev. Lett. 86 (2001) 4163–4166, http://dx.doi.org/10.1103/PhysRevLett.86.4163.
[20] S.L. Anna, N. Bontoux, H.A. Stone, Formation of dispersions using flow focusing in microchannels, Appl. Phys. Lett. 82 (2003) 364–366, http://dx.doi.org/10.1063/1.1537519.
[21] X. Casadevall i Solvas, A. deMello, Droplet microfluidics: recent developments and future applications, Chem. Commun. (Camb.) 47 (2011) 1936–1942, http://dx.doi.org/10.1039/c0cc02474k.
[22] H. Song, J.D. Tice, R.F. Ismagilov, A microfluidic system for controlling reaction networks in time, Angew. Chem. – Int. Ed. 42 (2003) 768–772, http://dx.doi.org/10.1002/anie.200390203.
[23] F. Sarrazin, L. Prat, N. Di Miceli, G. Cristobal, D.R. Link, D.a. Weitz, Mixing characterization inside microdroplets engineered on a microcoalescer, Chem. Eng Sci. 62 (2007) 1042–1048, http://dx.doi.org/10.1016/j.ces.2006.10.013.
[24] M.R. Bringer, C.J. Gerdts, H. Song, J.D. Tice, R.F. Ismagilov, Microfluidic systems for chemical kinetics that rely on chaotic mixing in droplets, Phil. Trans. R. Soc. Lond. A 108 (2004) 7–110.
[25] Y.-C. Tan, J.S. Fisher, A.I. Lee, V. Cristini, A.P. Lee, Design of microfluidic channel geometries for the control of droplet volume, chemical concentration, and sorting, Lab Chip 4 (2004) 292–298, http://dx.doi.org/10.1039/b403280m.
[26] Y.-C. Tan, Y.L. Ho, A.P. Lee, Microfluidic sorting of droplets by size, Microfluid Nanofluidics 4 (2008) 343–348, http://dx.doi.org/10.1007/s10404-007-0184-1.
[27] L.M. Fidalgo, C. Abell, W.T.S. Huck, Surface-induced droplet fusion in microfluidic devices, Lab Chip 7 (2007) 984–986, http://dx.doi.org/10.1039/b708091c.
[28] L.-H. Hung, K.M. Choi, W.-Y. Tseng, Y.-C. Tan, K.J. Shea, A.P. Lee, Alternating droplet generation and controlled dynamic droplet fusion in microfluidic device for CdS nanoparticle synthesis, Lab Chip 6 (2006) 174, http://dx.doi.org/10.1039/b513908b.
[29] Y.-C. Tan, Y.L. Ho, A.P. Lee, Droplet coalescence by geometrically mediated flow in microfluidic channels, Microfluid Nanofluidics 3 (2007) 495–499, http://dx.doi.org/10.1007/s10404-006-0136-1.
[30] D.R. Link, S.L. Anna, D.A. Weitz, H.A. Stone, Geometrically mediated breakup of drops in microfluidic devices, Phys. Rev. Lett. 92 (2004) 54503, http://dx.doi.org/10.1103/PhysRevLett.92.054503.
[31] P. Garstecki, H.A. Stone, G.M. Whitesides, Mechanism for flow-rate controlled breakup in confined geometries: a route to monodisperse emulsions, Phys. Rev. Lett. 94 (2005) 1–4, http://dx.doi.org/10.1103/PhysRevLett.94.164501.
[32] P. Garstecki, I. Gitlin, W. Diluzio, G.M. Whitesides, E. Kumacheva, H.A. Stone, Formation of monodisperse bubbles in a microfluidic flow-focusing device, Appl. Phys. Lett. 85 (2004) 2649–2651, http://dx.doi.org/10.1063/1.1796526.
[33] M.A. Herrada, A.M. Gañán-Calvo, J.M. López-Herrera, Generation of small mono-disperse bubbles in axisymmetric T-junction: the role of swirl, Phys. Fluids 23 (2011), http://dx.doi.org/10.1063/1.3610384.
[34] M. Hashimoto, S.S. Shevkoplyas, B. Zaso??ska, T. Szymborski, P. Garstecki, G.M. Whitesides, Formation of bubbles and droplets in parallel, coupled flow-focusing geometries, Small 4 (2008) 1795–1805, http://dx.doi.org/10.1002/smll.200800591.
[35] E. Talu, K. Hettiarachchi, R.L. Powell, A.P. Lee, P.A. Dayton, M.L. Longo, Maintaining monodispersity in a microbubble population formed by flow-focusing, Langmuir 24 (2008) 1745–1749, http://dx.doi.org/10.1021/la703065v.
[36] K. Hettiarachchi, E. Talu, M.L. Longo, P.A. Dayton, A.P. Lee, On-chip generation of microbubbles as a practical technology for manufacturing contrast agents for ultrasonic imaging, Lab Chip 7 (2007) 463, http://dx.doi.org/10.1039/b701481n.
[37] J. Wan, A. Bick, M. Sullivan, H.A. Stone, Controllable microfluidic production of microbubbles in water-in-oil emulsions and the formation of porous microparticles, Adv. Mater. 20 (2008) 3314–3318, http://dx.doi.org/10.1002/adma.200800628.
[38] A. Gañán-Calvo, Generation of steady liquid microthreads and micron-sized monodisperse sprays in gas streams, Phys. Rev. Lett. 80 (1998) 285–288, http://dx.doi.org/10.1103/PhysRevLett.80.285.
[39] M.A. Herrada, A.M. Gañán-Calvo, A. Ojeda-Monge, B. Bluth, P. Riesco-Chueca, Liquid flow focused by a gas: jetting, dripping, and recirculation, Phys. Rev. E – Stat. Nonlinear Soft Matter Phys. 78 (2008) 1–16, http://dx.doi.org/10.1103/PhysRevE.78.036323.
[40] J.M. Gordillo, M. Pérez-Saborid, A.M. Gañán-Calvo, Linear stability of co-flowing liquid–gas jets, J. Fluid Mech. 448 (2001) 23–51, http://dx.doi.org/10.1017/S0022112001005729.
[41] E.J. Vega, J.M. Montanero, M.A. Herrada, A.M. Gañán-Calvo, Global and local instability of flow focusing: the influence of the geometry, Phys. Fluids 22 (2010) 1–10, http://dx.doi.org/10.1063/1.3450321.
[42] L. Martín-Banderas, M. Flores-Masquera, P. Riesco-Chueca, A. Rodríguez-Gil, Á. Cebolla, S. Chávez, A.M. Gañán-Calvo, Flow focusing: a versatile technology to produce size-controlled and specific-morphology microparticles, Small 1 (2005) 688–692, http://dx.doi.org/10.1002/smll.200500087.
[43] C.H. Hidrovo, F.-M. Wang, J.E. Steinbrenner, E.S. Lee, S. Vigneron, C.-H. Cheng, J.K. Eaton, K.E. Goodson, Water slug detachment in two-phase hydrophobic microchannel flows, in: Proc. ICMM2005 3rd Int. Conf., Microchannels Minichannels, 2005, pp. 1–7, http://dx.doi.org/10.1115/icmm2005-75261.
[44] M.J. Cheah, I.G. Kevrekidis, J.B. Benziger, Water slug to drop and film transitions in gas-flow channels, Langmuir 29 (2013) 15122–15136, http://dx.doi.org/10.1021/la403057k.
[45] M.J. Cheah, I.G. Kevrekidis, J.B. Benziger, Water slug formation and motion in gas flow channels: the effects of geometry, surface wettability, and gravity, Langmuir 29 (2013) 9918–9934, http://dx.doi.org/10.1021/la4011967.
[46] B. Carroll, C. Hidrovo, Droplet detachment mechanism in a high-speed gaseous microflow, J. Fluids Eng. 135 (2013) 71206, http://dx.doi.org/10.1115/1.4024057.
[47] M. Mastiani, B. Mosavati, M. (Mike) Kim, Numerical simulation of high inertial liquid-in-gas droplet in a T-junction microchannel, RSC Adv. 7 (2017) 48512–48525, http://dx.doi.org/10.1039/C7RA09710G.
[48] X. Zhu, P.C. Sui, N. Djilali, Numerical simulation of emergence of a water droplet from a pore into a microchannel gas stream, Microfluid Nanofluidics 4 (2008) 543–555, http://dx.doi.org/10.1007/s10404-007-0209-9.
[49] A. Shahriari, M.M. Kim, S. Zamani, N. Phillip, B. Nasouri, C.H. Hidrovo, Flow regime mapping of high inertial gas–liquid droplet microflows in flow-focusing geometries, Microfluid Nanofluidics 20 (2016) 20, http://dx.doi.org/10.1007/s10404-015-1671-4.
[50] P. Tirandazi, C.H. Hidrovo, Liquid-in-gas droplet microfluidics; experimental characterization of droplet morphology, generation frequency, and monodispersity in a flow-focusing microfluidic device, J. Micromech. Microeng. 27 (2017) http://iopscience.iop.org/article/10.1088/1361-6439/aa7595/meta.
[51] P. Tirandazi, C.H. Hidrovo, Experimental investigation of geometrical parameters for gas-liquid droplet generation in flow-focusing configurations, in: ASME 13th Int. Conf. Nanochannels, Microchannels, Minichannels, ICNMM 2015, Collocated with ASME 2015, Int. Tech. Conf. Exhib. Packag. Integr. Electron. Photonic Microsystems (2015), http://dx.doi.org/10.1115/ICNMM2015-48834.
[52] P. Tirandazi, C.H. Hidrovo, Generation of uniform liquid droplets in a Microfluidic chip using a high-speed gaseous Microflow, in: ASME 14th Int. Conf. Nanochannels, Microchannels, Minichannels, ICNMM 2016, Collocated with ASME 2016 Heat Transf. Summer Conf. ASME 2016, Fluids Eng. Div Summer Meet. (2016), http://dx.doi.org/10.1115/ICNMM2016-8061.
[53] P. Tirandazi, G. Tomic, C.H. Hidrovo, An Ultra-High-Throughput Flow-Focusing Microfluidic Device for Creation of Liquid Droplets in Air, in: in: Proc. ASME 201, Int. Conf. Nanochannels, Microchannels, Minichannels, ICNMM2017, 2017, http://dx.doi.org/10.1115/ICNMM2017-5552, p. V001T03A003.
[54] K. Jiang, A.X. Lu, P. Dimitrakopoulos, D.L. DeVoe, S.R. Raghavan, Microfluidic generation of uniform water droplets using gas as the continuous phase, J. Colloid Interface Sci. 448 (2015) 275–279, http://dx.doi.org/10.1016/j.jcis.2015.02.023.
[55] B.D. Piorek, S.J. Lee, J.G. Santiago, M. Moskovits, S. Banerjee, C.D. Meinhart, Free-surface microfluidic control of surface-enhanced Raman spectroscopy for the optimized detection of airborne molecules, Proc. Natl. Acad. Sci. U. S. A. 104 (2007) 18898–18901, http://dx.doi.org/10.1073/pnas.0708596104.
[56] B.D. Piorek, S.J. Lee, M. Moskovits, C.D. Meinhart, Free-surface microfluidics/surface-enhanced Raman spectroscopy for real-time trace vapor detection of explosives, Anal. Chem. 84 (2012) 9700–9705, http://dx.doi.org/10.1021/ac302497y.
[57] B.D. Piorek, C. Andreou, M. Moskovits, C.D. Meinhart, Discrete free-surface millifluidics for rapid capture and analysis of airborne molecules using surface-enhanced Raman spectroscopy, Anal. Chem. 86 (2014) 1061–1066, http://dx.doi.org/10.1021/ac402628t.
[58] A.J. Alvarez, M.P. Buttner, L.D. Stetzenbach, PCR for bioaerosol monitoring: sensitivity and environmental interference, Appl. Environ. Microbiol. 61 (1995) 3639–3644 http://www.pubmedcentral.nih.gov/articlerender.fcgi?artid=167662&tool=pmcentrez&rendertype=abstract.
[59] J.S. West, S.D. Atkins, J. Emberlin, B.D.L. Fitt, PCR to predict risk of airborne disease, Trends Microbiol. 16 (2008) 380–387, http://dx.doi.org/10.1016/j.tim.2008.05.004.
[60] D. Hospodsky, N. Yamamoto, J. Peccia, Accuracy, precision, and method detection limits of quantitative PCR for airborne bacteria and fungi, Appl. Environ. Microbiol. 76 (2010) 7004–7012, http://dx.doi.org/10.1128/AEM.01240-10.
[61] J. Peccia, M. Hernandez, Incorporating polymerase chain reaction-based identification, population characterization, and quantification of microorganisms into aerosol science: a review, Atmos. Environ. 40 (2006) 3941–3961, http://dx.doi.org/10.1016/j.atmosenv.2006.02.029.
[62] G. Pardon, L. Ladhani, N. Sandström, M. Ettori, G. Lobov, W. Van Der Wijngaart, Aerosol sampling using an electrostatic precipitator integrated with a microfluidic interface, Sens. Actuators B Chem. 212 (2015) 344–352, http://dx.doi.org/10.1016/j.snb.2015.02.008.
[63] D. Verreault, S. Moineau, C. Duchaine, Methods for sampling of airborne viruses, Microbiol. Mol. Biol. Rev. 72 (2008) 413–444, http://dx.doi.org/10.1128/MMBR.00002-08.

[64] J.D. Greenwood, Y. Liu, D.E. Busacker, D. Cheng, H. Jiang, Collection of gaseous and aerosolized samples using microfluidic devices with Gas-liquid interfaces, IEEE Sens. J. 10 (2010) 952–959, http://dx.doi.org/10.1109/JSEN.2009.2038071.
[65] S. Kaneda, K. Ono, T. Fukuba, T. Nojima, T. Yamamoto, T. Fujii, Modification of the glass surface property in PDMS-glass hybrid microfluidic devices, Anal. Sci. 28 (2012) 39, http://dx.doi.org/10.2116/analsci.28.39.
[66] T. Fu, Y. Wu, Y. Ma, H.Z. Li, Droplet formation and breakup dynamics in microfluidic flow-focusing devices: from dripping to jetting, Chem. Eng. Sci. 84 (2012) 207–217, http://dx.doi.org/10.1016/j.ces.2012.08.039.
[67] S. van Loo, S. Stoukatch, M. Kraft, T. Gilet, Droplet formation by squeezing in a microfluidic cross-junction, Microfluid Nanofluidics 20 (2016) 146, http://dx.doi.org/10.1007/s10404-016-1807-1.
[68] P. Garstecki, M.J. Fuerstman, H. a Stone, G.M. Whitesides, Formation of droplets and bubbles in a microfluidic T-junction-scaling and mechanism of break-up, Lab Chip 6 (2006) 437–446, http://dx.doi.org/10.1039/b510841a.
[69] X. Chen, T. Glawdel, N. Cui, C.L. Ren, Model of droplet generation in flow focusing generators operating in the squeezing regime, Microfluid Nanofluidics 18 (2015) 1341–1353, http://dx.doi.org/10.1007/s10404-014-1533-5.
[70] T. Glawdel, C.L. Ren, Droplet formation in microfluidic T-junction generators operating in the transitional regime. I Experimental observations, Phys. Rev. E – Stat. Nonlinear, Soft Matter Phys. 86 (2012) 1–9, http://dx.doi.org/10.1103/PhysRevE.86.026308.
[71] T. Glawdel, C.L. Ren, Droplet formation in microfluidic T-junction generators operating in the transitional regime. II. Modelling, Phys. Rev. E – Stat. Nonlinear, Soft Matter Phys. 86 (2012) 1–12, http://dx.doi.org/10.1103/PhysRevE.86.026308.
[72] J. Wang, Y. Li, X. Wang, J. Wang, H. Tian, P. Zhao, Y. Tian, Y. Gu, L. Wang, C. Wang, Droplet microfluidics for the production of microparticles and nanoparticles, Micromachines 8 (2017) 1–23, http://dx.doi.org/10.3390/mi8010022.
[73] C.N. Baroud, F. Gallaire, R. Dangla, Dynamics of microfluidic droplets, Lab Chip 10 (2010) 2032–2045, http://dx.doi.org/10.1039/c001191f.
[74] G.F. Christopher, S.L. Anna, Microfluidic methods for generating continuous droplet streams, J. Phys. D Appl. Phys. 40 (2007) R319–R336, http://dx.doi.org/10.1088/0022-3727/40/19/R01.
[75] E. Delamarche, H. Schmid, B. Michel, H. Biebuyck, Stability of molded polydimethylsiloxane microstructures, Adv. Mater. 9 (1997) 741–746, http://dx.doi.org/10.1002/adma.19970090914.
[76] D. Qin, Y. Xia, G.M. Whitesides, Soft lithography for micro- and nanoscale patterning, Nat. Protoc. 5 (2010) 491–502, http://dx.doi.org/10.1038/nprot.2009.234.
[77] Y. Xia, G.M. Whitesides, Soft lithography, Annu. Rev. Mater. Sci. 28 (1998) 153–184.
[78] T. Gervais, J. El-Ali, A. Günther, K.F. Jensen, Flow-induced deformation of shallow microfluidic channels, Lab Chip 6 (2006) 500–507, http://dx.doi.org/10.1039/b513524a.
[79] R. Dangla, F. Gallaire, C.N. Baroud, Microchannel deformations due to solvent-induced PDMS swelling, Lab Chip 10 (2010) 2972–2978, http://dx.doi.org/10.1039/c003504a.
[80] J.N. Lee, C. Park, G.M. Whitesides, Solvent compatibility of poly(dimethylsiloxane)-based microfluidic devices, Anal. Chem. 75 (2003) 6544–6554, http://dx.doi.org/10.1021/ac0346712.
[81] M. Kim, Y. Huang, K. Choi, C.H. Hidrovo, The improved resistance of PDMS to pressure-induced deformation and chemical solvent swelling for microfluidic devices, Microelectron. Eng. 124 (2014) 66–75, http://dx.doi.org/10.1016/j.mee.2014.04.041.
[82] B. Timmer, W. Olthuis, A. Van Den Berg, Ammonia sensors and their applications – a review, Sens. Actuators B Chem. 107 (2005) 666–677, http://dx.doi.org/10.1016/j.snb.2004.11.054.
[83] B.P. LeClair, A.E. Hamielec, H.R. Pruppacher, W.D. Hall, A theoretical and experimental study of the internal circulation in water drops falling at terminal velocity in air, J. Atmos. Sci. 29 (1972) 728–740, http://dx.doi.org/10.1175/1520-0469(1972)029<0728:ATAESO>2.0. CO;2.
[84] H. Amokrane, B. Caussade, Gas absorption into a moving spheroidal water drop, J. Atmos. Sci. 56 (1999) 1808–1829, http://dx.doi.org/10.1175/1520-0469(1999)056<1808:GAIAMS>2.0.CO;2.
[85] W.H. Chen, Atmospheric ammonia scavenging mechanisms around a liquid droplet in convective flow, Atmos. Environ. 38 (2004) 1107–1116, http://dx.doi.org/10.1016/j.atmosenv.2003.11.013.
[86] Y. Huangs, M. Lu, Continuous phase mass transfer coefficients for single droplets moving in an infinite, Chem. Eng. Commun. 6445 (2007) 37–41, http://dx.doi.org/10.1080/00986449908912756.
[87] T. Elperin, A. Fominykh, Conjugate mass transfer during gas absorption by falling liquid droplet with internal circulation, Atmos. Environ. 39 (2005) 4575–4582, http://dx.doi.org/10.1016/j.atmosenv.2005.04.005.

Biographies

Pooyan Tirandazi is a Ph.D. candidate and research assistant in Multiscale Thermal Fluids Laboratory (MTFL) in the Mechanical and Industrial Engineering Department at Northeastern University. He received his Bachelor's degree in Mechanical Engineering from Sharif University of Technology (Tehran, Iran). His research focuses on the investigation of droplet generation and entrainment in high-speed gaseous microflows towards developing novel Lab-on-a-Chip systems for gas-based biochemical sensing and material synthesis. He has also actively worked on microfabrication techniques for microfluidics, and numerical simulation for multiphase flows.

Dr. Carlos Hidrovo is an assistant professor in the Mechanical and Industrial Engineering Department at Northeastern University. He earned his Ph.D. in Mechanical Engineering from the Massachusetts Institute of Technology. Prior to joining Northeastern, Dr. Hidrovo held professional appointments at MIT, Stanford University, and The University of Texas at Austin. He is the recipient of an NSF CAREER Award from the Fluid Dynamics program, a DARPA Young Faculty Award from the Microsystems Technology Office (MTO), and an ASME Robert T. Knapp Award. Dr. Hidrovo research interests lie at the intersection of multiscale and multiphase flow and transport phenomena, surface tension interactions in micro/nanoengineered structures, and electrokinetic ion transport in porous media for applications in energy storage, portable biochemical diagnostics, thermal management, and water treatment systems. He is also actively involved in developing novel imaging and diagnostic tools in these areas.